ICEF2022-90999

Investigations into the Performance and Emissions Characteristics of FT Synthetic Aviation Fuel, Isoparaffinic Kerosene (IPK), in a Single-Cylinder **Indirect Injection (IDI) Engine**

Valentin Soloiu¹, Amanda Weaver¹, Lily Parker¹, Richard Smith III¹, Austin Brant¹, Dillan Brock¹, Marcel Ilie¹

¹Georgia Southern University, Combustion Laboratory, Statesboro, GA

ABSTRACT

In this study, iso-paraffinic kerosene (IPK) was analyzed for ignition delay, combustion delay, pressure trace, pressure rise rate and, apparent heat release rate in an experimental single cylinder indirect injection (IDI) compression ignition engine as well as in a constant volume combustion chamber (CVCC). Neat IPK, neat ULSD, and a bymass blend of 50%IPK50%ULSD were analyzed in a CVCC and an IDI engine to determine the effect of Derived Cetane Number (DCN), Ignition Delay (ID), and Low Temperature Heat Release (LTHR) on combustion timing and engine knock.

In the CVCC, IPK was found to have a significantly lower DCN than ULSD at 26 and 47, respectively. The blend was found to have a DCN between the two neat fuels at 37.5. Additionally, the ignition delay increased in the CVCC from 3.56 ms for ULSD to 5.3 ms for IPK with the blend falling between the two at 4.38 ms.

For engine research, the single-cylinder experimental IDI engine was run at 2400 rpm at 5, 6, and 7 Indicated Mean Effective Pressure (IMEP) using each of the three researched fuels. It was found that when running neat IPK, there was a profound level of engine knock at all loads characterized by the 60% increase in the Peak Pressure Rise Rate (PPRR) when compared to ULSD. The pressure trace for IPK at all loads showed a significant delay in combustion due to IPK's resistance to autoignition. This was observed in the increasing ignition delay in the engine from 0.88 ms for ULSD to 1.1 ms at 7 bar IMEP for IPK. Despite the delay in ignition for IPK, all three researched fuels reached peak Apparent Heat Release Rate (AHRR) at approximately 370° leading to a much more rapid increase in AHRR for IPK when compared to ULSD. This steep slope in the AHRR, also seen in the increased PPRR, and longer ID caused the high levels of engine knock, observed as oscillations in the pressure trace which decreased in magnitude as IMEP increased.

NOMENCI ATURE

NONE	DIVIENCLATURE		
AFR	Air Fuel Ratio		
AHRR	Apparent Heat Release		
ATDC	After Top Dead Center		
BTDC	Before Top Dead Center		
BMEP	Break Mean Effective Pressure		
CAD	Crank Angle Degree		
CA10	Crank Angle Degree @ 10% mass burned		
CA50	Crank Angle Degree @ 50% mass burned		
CA90	Crank Angle Degree @ 90% mass burned		
CRDI	Common Rail Direct Injection		
CD	Combustion Delay		
CDC	Conventional Diesel Combustion		
CI	Compression Ignition		

CN	Cetane Number
CO	Carbon Monoxide
CVCC	Constant Volume Combustion Chambe
D	Engine Pore

ע	Engine Bore
DCN	Derived Cetane Number
DI	Direct Injection

Dv10	Largest Droplet Size of 10% of Fuel Spray
Dv50	Largest Droplet Size of 50% of Fuel Spray
Dv90	Largest Droplet Size of 90% of Fuel Spray

DTA	Differential Thermal Analysis
EPA	Environmental Protection Agency

1 1	Tisener Tropsen
FTIR	Fourier Transform Spectroscopy

Fischer-Tronsch

HC	Hydrocarbons
HHV	Higher Heating Value
HTHR	High Temperature Heat Releas
ID	Ignition Delay
IDI	Indirect Injection

וטו	mairect injection
IMEP	Indicated Mean Effective Pressure
IDIZ	Las Dansffinis Vanagana

IPK Iso-Paraffinic Kerosene LHV Lower Heating Value

FT

LTC Low Temperature Combustion LTHR Low Temperature Heat Release

N Engine Speed

NTCR Negative Temperature Coefficient Region

NOx Nitrogen oxides
PPRR Peak Pressure Rise Rate
Re Reynolds Number
RPM Revolutions Per Minute
RI Ringing Intensity

S Stroke

SMD Sauter Mean Diameter

TA10 Temperature @ 10% mass vaporized TA50 Temperature @ 50% mass vaporized TA90 Temperature @ 90% mass vaproized

TGA Thermogravimetric Analysis
UHC Unburnt Hydrocarbons
ULSD Ultra-Low Sulfur Diesel

INTRODUCTION

With the growing concern of fossil fuel availability, there is a building pressure to find alternative fuel sources. This shrinking availability of fossil fuels is further exemplified as the aerospace field continues to grow. Though there have been significant developments made in electric vehicle technology, years of work remain before the infrastructure and battery science and technology can support a global transition to entirely electric power [1]. More immediate solutions to the growing problem involve the development and implementation of alternative fuels for use in conventional Compression Ignition (CI) engines as a drop-in replacement. Several innovative processes have been developed which can create synthetic fuels capable of replacing liquid petroleum fuels.

One such process used in the development of alternative fuels is the Fischer-Tropsch process. Invented in the 1920's, the process converts hydrocarbon sources such as coal, natural gas, or biomass into synthetic, ultra-pure fuels [2]. One such fuel is Iso-Paraffinic Kerosene (IPK) derived from coal. IPK has been investigated in its neat form in the Constant Volume Combustion Chamber and in a turbojet engine and analyzed for emissions, noise, vibration, and harshness (NVH), and thermal efficiency. It was found to reduce NO, UHC, and CO emissions with an increase in the CO₂ emissions and NVH signature while increasing thermal efficiency [3-9].

These fuels generally contain minimal aromatics and a near zero sulfur content. The low levels of these two components reduce the lubricity, viscosity, and heat of vaporization of the fuel [10]. The lower heat of vaporization indicated that the fuel would form a homogeneous air fuel mixture more rapidly than USLD.

In this study, an analysis of the thermophysical properties as well as a complete determination of the combustion characteristics of IPK when compared to a baseline of ULSD was conducted in both a CVCC and an Indirect Injection (IDI) Compression Ignition (CI) engine. This investigation is conducted with the objective to determine the performance and viability of this synthetic fuel as an alternative or a blend for use in common CI engines. This research focuses on the knocking

events associated with fuels of a lower DCN and emissions output from a single-cylinder, IDI through a swirl chamber.

THERMOPHYSICAL PROPERTIES

Investigations were conducted on the thermophysical properties of neat ULSD and IPK. These properties provide context for the combustion behavior of each of the researched fuels in both the CVCC and in the CI engine. Most notable are the thermogravimetric analysis, differential thermal analysis, and the spray atomization and droplet distribution. Spray pattern formation and vaporization rate play a key role in the development of the air fuel mixture [11-14]. From this determination, it was found that the thermophysical properties for IPK are apparently more favorable for combustion when compared to ULSD. The Derived Cetane Number (DCN), Ignition Delay (ID), and the Combustion Delay (CD) as well as important thermophysical properties are displayed in Table 1. These values and determinations will be further discussed in the following chapters.

Table 1: Thermophysical Properties of Neat Researched Fuels

	ULSD	IPK
LHV (MJ/kg)	41.1	44.25
DCN*	47	25.88
Avg. ID (ms)	3.56	5.3
Avg. CD (ms)	5.15	17.2
Viscosity @ 40°C (cP)	2.44	1.02
SMD [µm]	22.36	14.96

Table 2: Chemical Composition for ULSD and IPK [15,16]

Composition	ULSD	Sasol IPK
n-Paraffins (wt%)	25.50	2.1
Iso-paraffins (wt%)	25-50	88
Cyclo-paraffins (wt%)	20-40	9
Aromatics (wt%)	15-40	< 0.5
Total sulfur (wt%)	Max 0.05	< 0.001

Shown in Table 2 are the hydrocarbon and paraffin distributions for ULSD#2 and IPK. The chemical composition of the fuel gives insight into the thermophysical properties, combustion characteristics, and emissions profile. In this investigation, ULSD and IPK were analyzed for viscosity, heat of combustion, volatility, and spray characteristics. Heat of combustion and viscosity were determined using a Parr 1341 constant volume calorimeter and a Brookfield DV-II +Pro rotational viscometer, respectively. The Lower Heating Value (LHV) and the viscosity at 40°C can be found in Table 1.

Low Temperature Oxidation and Thermal Stability

A differential thermal analysis (DTA) and the thermogravimetric analysis (TGA) were conducted for each of the neat fuels. The analysis was conducted using a Shimadzu DTG-60. A sample of each researched fuel weighing approximately 10 mg was placed in the furnace then heated from 20 °C to 600 °C at a rate of 20 °C per minute. A constant airflow of 15 mL/min was used to purge the furnace.

For calibration, a baseline is placed in the furnace alongside the fuel sample. The baseline used for this experimentation is an inert alumina powder. The alumina powder is chosen as it loses little to no mass as the chamber is heated.

The TGA is a measurement of the rate of vaporization in terms of the percent reduction in mass as a function of temperature and indicates the volatility of the fuel. The DTA is a measurement of the endothermic and exothermic reactions of the fuel as the temperature is increased.

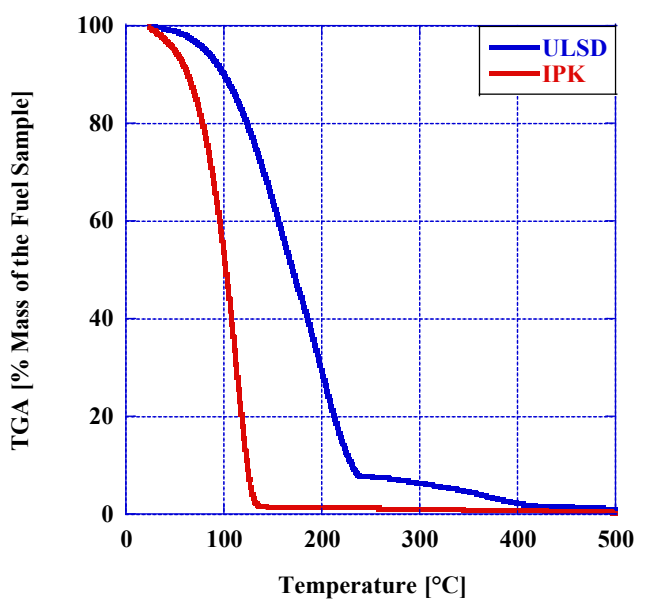


Figure 1: TGA of Neat ULSD and IPK

The TGA in Figure 1 shows IPK reducing its mass sample at a significantly faster rate than that of ULSD indicating IPK has a much higher volatility than that of ULSD. A fuel with a higher volatility after injection fuel forms a homogeneous air fuel ratio at a lower temperature due to its rapid vaporization rate [17,18]. Table 3 represents the key numbers to quickly quantify the vaporization rate.

These temperature values are taken when 10%, 50%, and 90% of the fuel's initial mass is vaporized and are denoted as TA10, TA50, and TA90. It was found that the values for IPK and ULSD at TA10 were much closer at 71.7 °C and 100°C, respectively, than the temperature for each fuel for TA90 at 131.2 °C and 230.2 °C, respectively. This is a further indication of the higher volatility of IPK over ULSD.

Table 3: Thermogravimetric Analysis (TGA)

	ULSD	IPK
TA (10) °C	100.0	71.7
TA (50) °C	170.0	108.1
TA (90) °C	230.2	131.2

Figure 2 shows the DTA of the researched fuels and represents the energy which is absorbed and released as the temperature is increased. These endothermic and exothermic reactions can be seen as negative and positive slopes respectively. The magnitude of the slope indicates the rate at which this energy is absorbed and released.

Similar to the graph of the TGA, IPK absorbs and releases its energy at a lower temperature and at a faster rate than ULSD. Additionally, ULSD has a second section of endothermic and exothermic reactions at approximately 400 °C. Conversely, the DTA for IPK shows that there are two additional sections of exothermic and endothermic reactions of a significantly lower magnitude. This difference in the DTA of IPK and ULSD can be attributed to the hydrocarbon weight and the volatility of component species and low temperature oxidation rates. Heavier hydrocarbons tend to have a lower vaporization rate and a higher boiling point than lighter hydrocarbons. As shown in Table 2, IPK is primarily comprised of unsaturated, branch chain isoparaffins. This composition contributes to the overall increase in the fuel's volatility.

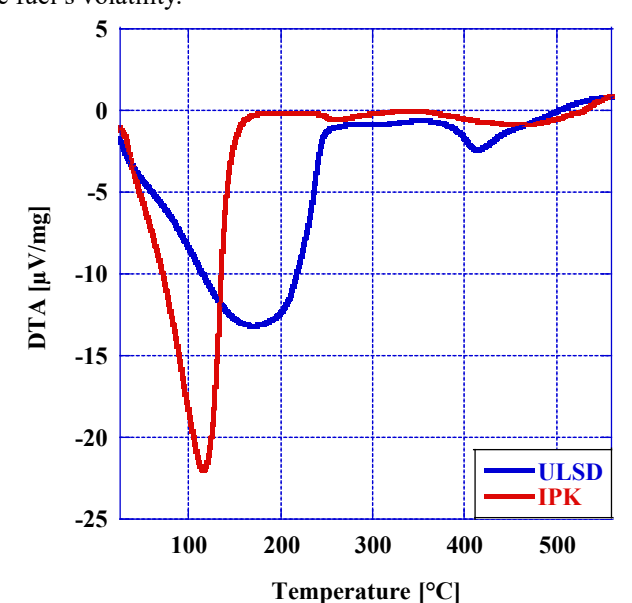


Figure 2: DTA of IPK and ULSD

Spray Atomization, Droplet Distribution, and Mixture Formation investigations with a Mie Scattering He-Ne Laser Apparatus

An analysis was conducted on the spray atomization, droplet distribution, and mixture formation of each of the researched fuels using a Malvern Spraytec He-Ne laser. This apparatus is shown in Figure 3. Fuels were injected 100mm away

from the laser beam at a pressure of 180 bar. Data was taken from 28 of the 36 light detectors at a rate of 10kHz and recorded from 0.1 ms before the trigger to 5 ms after the trigger. The recorded data is then interpreted using Mie Scattering and Fraunhofer diffraction theory to determine the Sauter Mean Diameter (SMD) of the spray droplets due to the diffraction of the laser.

This calculation is determined using two equations for the scattering of unpolarized light by a spherical droplet. This correlation is shown in Equation 1 [19].

$$I(\theta) = \frac{I_0}{2k^2a^2}([S_1(\theta)]^2 + [S_2(\theta)]^2)$$
 (1)

In this correlation, $I(\theta)$ is the light intensity after scattering as a function of the angle θ at which the light hits the droplet relative to where it is detected. Initial intensity of the beam is I_0 where k is the wavenumber, in $2\pi/\lambda$, and a is the distance between the light source and the receiving detector. $S_1(\theta)$ and $S_2(\theta)$ are dimensionless, complex functions describing the change of amplitude in the perpendicular and the parallel polarized light.

Fraunhofer diffraction theory does not rely on the optical properties of the droplet allowing for more practical application of the theory in a wider variety of different mixtures and shapes. The correlation associated with this theory is listed in Equation 2 [19]. This equation uses the same $I(\theta)$ and k values but also includes the dimensionless size parameter $\alpha = \pi x/\lambda$ using x as the particle size.

$$I(\theta) = \frac{I_0}{2k^2 a^2} \alpha^4 \left(\frac{J_I(\alpha \sin(\theta))}{\alpha \sin \theta} \right)$$
 (2)

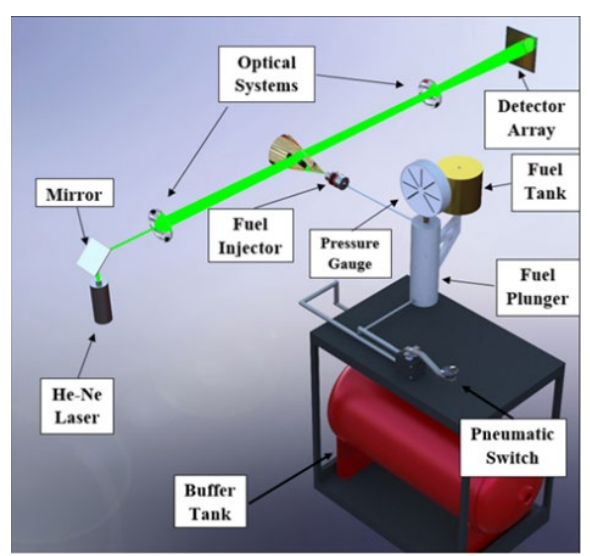


Figure 3: Malvern Spraytec Apparatus [20]

For each of the three researched fuels, averages were taken of both the droplet distribution and the SMD to create an accurate representation of the spray profile for each of the researched fuels. The results for this determination are shown in Figure 4. Due to the higher viscosity of ULSD over IPK, the droplet distribution is skewed toward a higher droplet diameter

when compared to IPK which had the lowest droplet size over the control volume in the spray. The SMD values of the blend of 50% ULSD and 50%IPK by mass fell between each of the neat fuels.

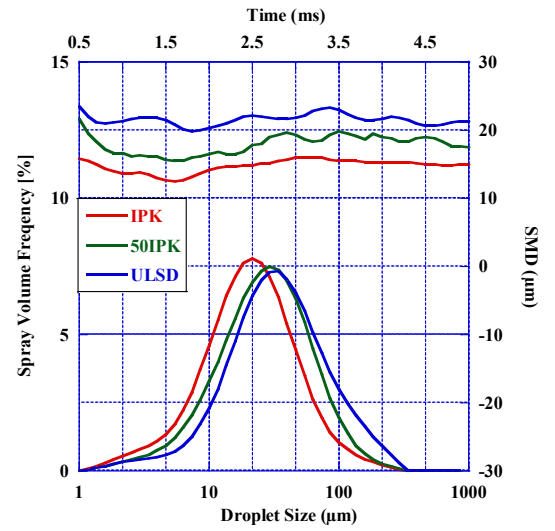


Figure 4: Spray Development for ULSD, 50IPK50ULSD, and IPK

CVCC Experimental Methods

For the CVCC experimentation, a Petroleum Analysis Company (PAC) CID 510 was used to determine the Ignition Delay (ID), Combustion Delay (CD), and the Derived Cetane Number (DCN) of the researched fuels. These values are an indication of the fuel's autoignition quality. The apparatus conducted 5 conditioning cycles of injection, combustion, and exhaust before taking measurements for 15 combustion cycles. Pressure data from each of the cycles is averaged for the 15 cycles to provide an accurate bank of data. These testing cycles follow the ASTM standard D7667-14.a represented in Table 4.

Table 4: ASTM D7668-14.a

Wall Temp.	Fuel Injection Pressure	Coolant Temp.	Injection Pulse Width	Chamber Pressure
595.5 °C	1000 bar	50 °C	2.5 ms	20 bar

A schematic of the external geometry and a cross section of the internal geometry of the combustion chamber is shown in Figure 5. In the cross-sectional view, component 1 is the high-pressure common rail and component 2 is the 6-oriface Bosch high-pressure fuel injector. Fuel is injected into a uniformly heated, constant volume, pressure-controlled combustion chamber labeled as component 2 in the external model of the system. Component 3 is the pressure sensor used to measure the increase in pressure due to combustion, chamber cooling due to fuel injection, and oscillations after peak pressure. Fuel line pressure is measured as well using component 4 in the diagram.

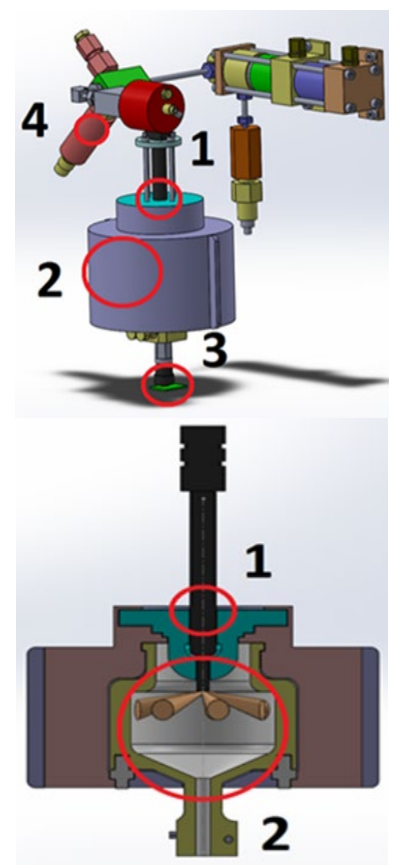


Figure 5:PAC CID 510 Constant Volume Combustion Chamber

The pressure trace from the combustion of ULSD, 50IPK50ULSD, and IPK are shown in Figure 6. The duration of combustion for IPK is much longer with a total combustion time of 19.32 ms when compared to ULSD at 3.64 ms. The blend then falls between the two neat fuels leaning more toward ULSD than IPK with a total combustion time of 8.36 ms. This observation is reflected in the DCN of each of the researched fuels. Additionally, the pressure rise rate for IPK is much lower than that of ULSD.

Pressure and Ringing Analysis

From the graph in Figure 6, it can be observed that there are ringing events around peak pressure present in ULSD, but not in 50ULSD50IPK and neat IPK. To compare pressure oscillations and to more closely investigate the ringing events. A zoom of the combustion pressure at its peak is shown in Figure 7. Additionally, to allow for careful observation of the pressure trace for all three researched fuels, the x-axis uses a logarithmic scale due to the late combustion of IPK. It was observed that with the addition of 50% by mass of IPK all the ringing events clearly present in ULSD around peak pressure disappear. This is due to the increase in the ID and CD contributing to a lower DCN.

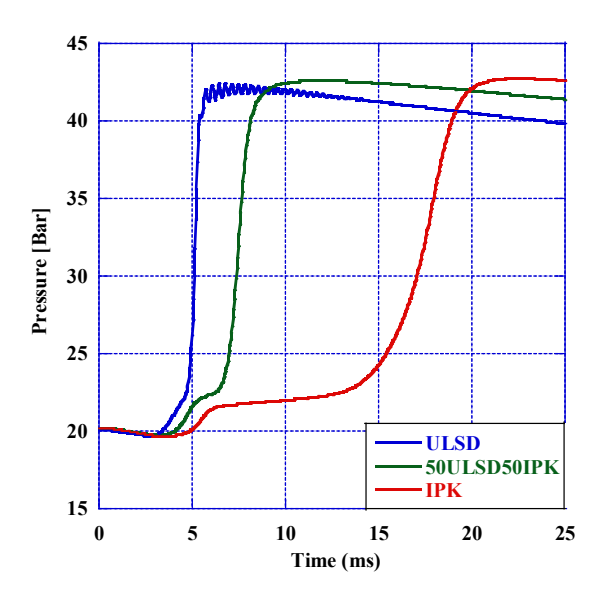


Figure 6: Pressure Traces for ULSD, 50ULSD50IPK, and IPK

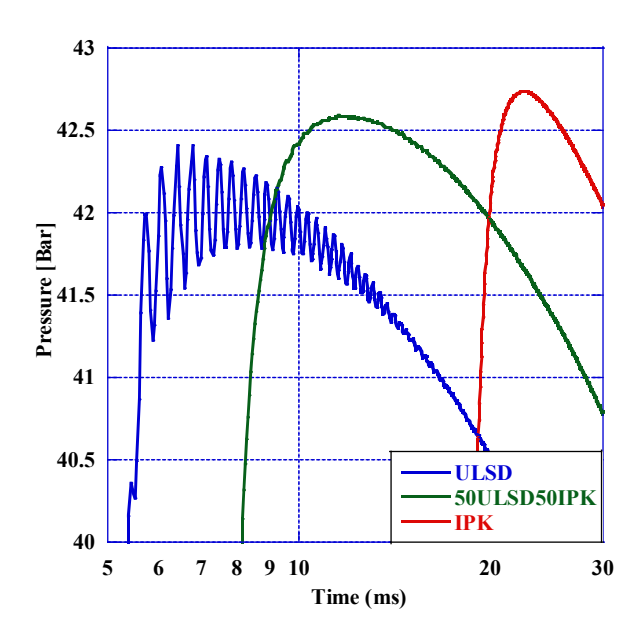


Figure 7: Peak Pressures with Logarithmic Scale

Table 5 illustrates the peak pressure for each of the researched fuels and the time from the start of injection at which it reached peak pressure. It was observed that while IPK reaches a higher peak pressure, there is a significantly longer combustion period when compared to ULSD.

Table 5: Peak Pressures and Time at Peak

Researched Fuel	ULSD	50IPK50ULSD	IPK
Time (ms)	6.44	11.56	22.6
Peak Pressure (bar)	42.41	42.58	42.73

Apparent Heat Release Rate (AHRR) and Low-Temperature Heat Release (LTHR) Regions

The Apparent Heat Release Rate or the AHRR is calculated from pressure and is used to identify the different regions of combustion. A graph of the AHRR for each of the researched fuels can be seen in Figure 8.

The governing equation for this calculation can be seen as Equation 3. This is modeled as a closed loop system in which heat transfer is neglected with the wall temperature maintained at 595.5°C. Time for the combustion cycle begins at 0.04 ms and global specific heat ratio is assumed to be the same for each of the 15 measured combustion cycles [21-24].

$$\frac{dQ}{dt} = \frac{1}{\gamma - 1} V \frac{dP}{dt} \tag{3}$$

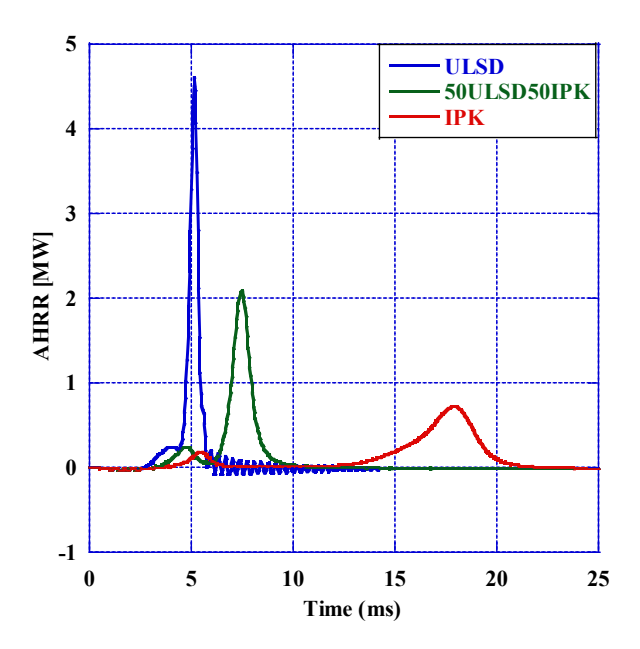


Figure 8: AHRR for ULSD, 50ULSD50IPK, and IPK

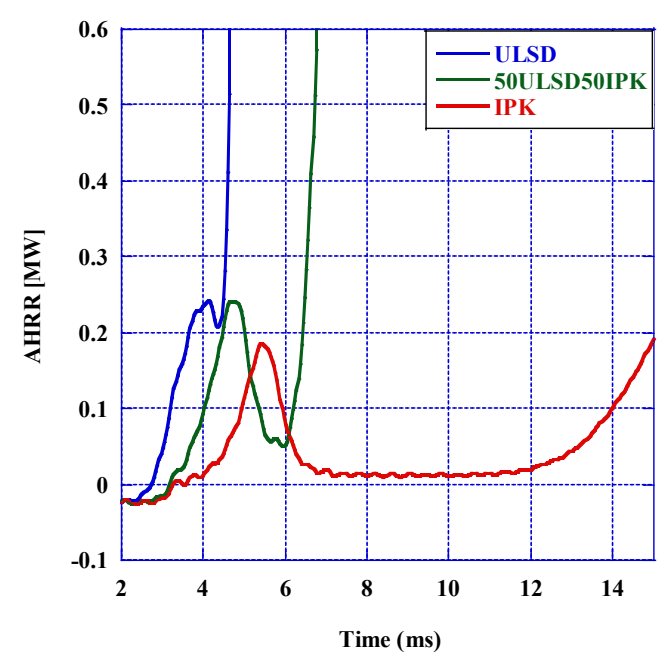


Figure 9: LTHR for ULSD, 50ULSD50IPK, and IPK

A zoom of the LTHR regions for each of the researched fuels is shown in Figure 9. This region is notable as it contains the region for which the initial cracking of hydrocarbon bonds creates the low-luminosity blue flames referred to as cool flames. After the period of cool flame formation, the formation of heavy peroxides, predominated by ketohydroperoxide, causes a decrease in the AHRR. This region is referred to as the Negative Temperature Coefficient Region (NTCR) and is the area of increasing temperature for which the slope of AHRR becomes negative.

The thermophysical properties of IPK indicate that the fuel will have better autoignition characteristics, however in the CVCC study on the combustion characteristics of IPK, it was found that IPK had poorer autoignition characteristics than ULSD with an extended ID and CD.

COMBUSTION ANALYSIS

This study investigates the performance characteristics of neat IPK and a by mass blend of 50% IPK and 50% ULSD in an Indirect Injection (IDI) engine when compared to neat ULSD. The engine was run at 2400 rpm and loads of 5, 6, and 7 bar Indicated Mean Effective Pressure (IMEP). The engine configuration can be seen in Figure 10 and the triple vortex precombustion chamber is shown in Figure 11. This engine is naturally aspirated, and liquid cooled.

Engine load and IMEP were controlled using an attached hydraulic dynamometer. Fuel is injected using a 1x0.200mm nozzle with a Pintaux needle. Detailed engine parameters are listed in Table 6.

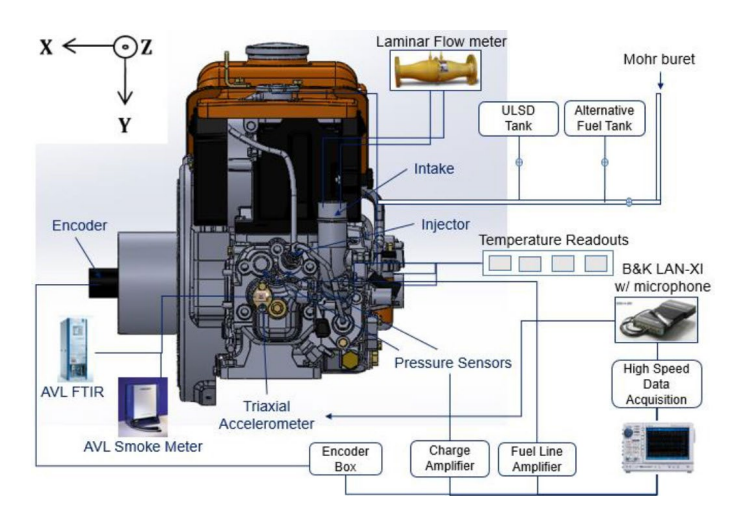


Figure 10: IDI Engine Configuration [26]

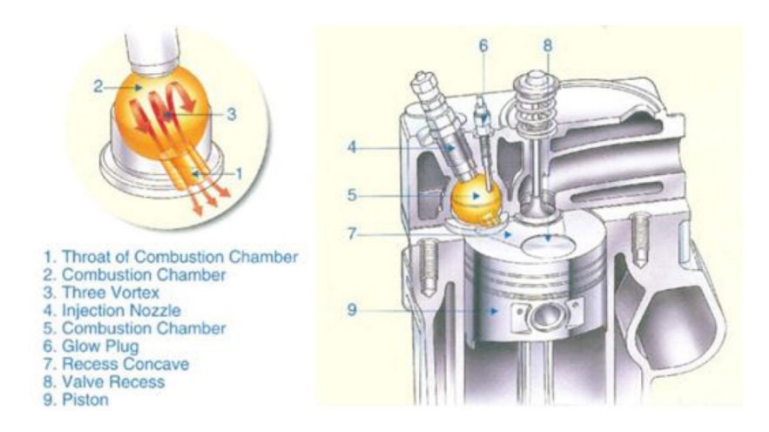


Figure 11: Triple Vortex Pre-Combustion Chamber [26]

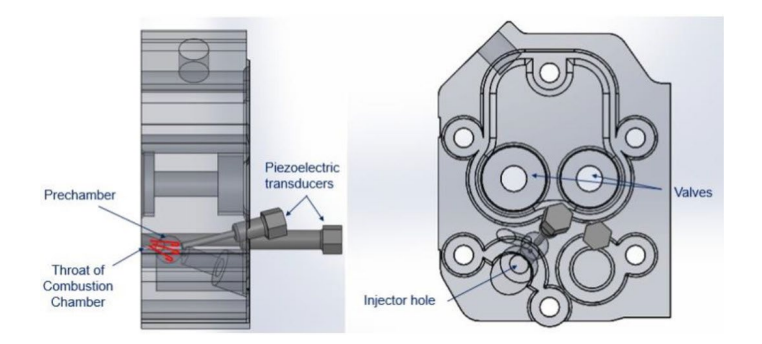


Figure 12: Cylinder Head Instrumentation with Pressure Sensor using Glow Plug Adaptor (Kistler type 6053 CC)

Table 6: IDI Engine Physical Specifications

Parameter	Value
Bore x Stroke	77mm x 70 mm
Displacement	0.35 L
Compression Ratio	23.5:1
Injection Nozzle	1 orifice x 0.20 mm
Injection Pressure	150 bar
Number of Cylinders	1
Engine Effective Power	5.2 kW

Combustion chamber pressure was measured using a Kistler 6053CC and fuel line pressure was measured using a Kistler type 6229 in-line injector pressure sensor. An Omron E6C2 rotary encoder was affixed to the crankshaft of the engine to determine CAD and TDC. Data from the pressure sensors was recorded using a Yokogawa DL850 high speed data acquisition system. Schematics of the engine configuration are shown in Figures 10-12.

Compression ignition engines undergo in general two heat release phases referred to in this study as premixed and diffusion burn. The rapid release of energy at the start of combustion and is primarily combusting the finely atomized droplets at the edge of the spray where the vaporization of the fuel around these droplets creates a more homogeneous air fuel mixture.

Because of the pre-combustion chamber configuration, there is a high level of turbulence and a high temperature in the separate combustion chamber the premixing is very violent. As seen in Figure 17, there is an initial spike in AHRR associated with the combustion of the fuel in the swirl chamber with a subsequent spike associated with combustion in the main combustion chamber. These heat release spikes indicate there are no diffusion flames for this engine configuration. This, in addition to the high fuel impingement, cause IDI engines to have a shorter ignition delay [26-30] and multifuel capability. While the spray break and vaporization properties are independent from the amount of energy produced from the premixed burn, air blended with the premixed fuel vapor has a significant impact on the peak heat release during combustion. Ignition delay also plays a crucial role in the peak heat release during combustion. The combustion chamber pressure and the fuel line pressure for ULSD, 50ULSD50IPK, and IPK are displayed in Figure 13.

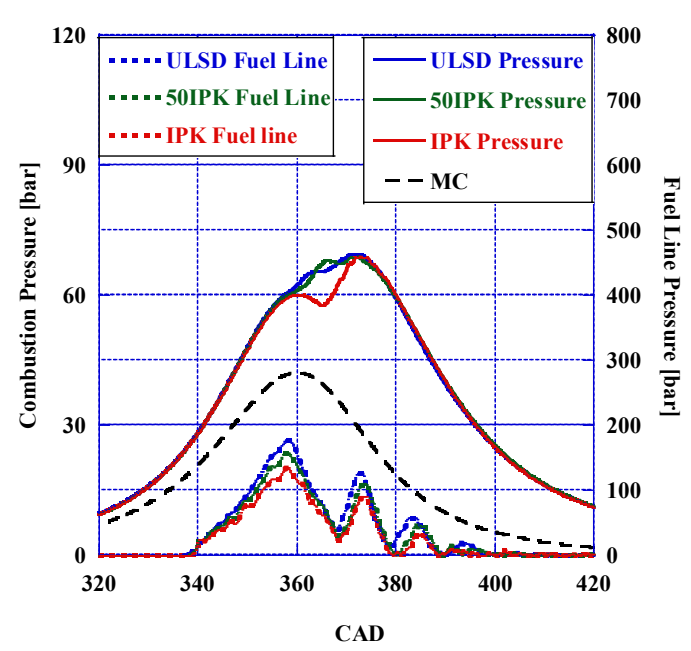


Figure 13: Combustion Pressure for ULSD, 50ULSD50IPK, and IPK at 7 Bar IMEP

Table 7: Peak Pressures at 7 bar IMEP

Researched Fuel	Peak Pressure bar/CAD
ULSD	69.5/370.98
50ULSD50IPK	68.9/372.42
IPK	68.9/372.78

Due to the low DCN and the extended ignition delay for IPK observed in the CVCC analysis of the fuels, it can be seen that there is a significant delay in combustion for IPK. IPK does not ignite until after TDC about the time when the air fuel mixture from the swirl chamber is drawn back into the main chamber above the piston. The extended ID and high volatility of IPK allow time for the complete vaporization of the spray providing quasi homogeneous conditions for combustion. Once ignition occurs, (after TDC) there is rapid burn with high Pressure Rise Rate (PRR) causing higher peak pressures and substantial knock as seen in Figures 16 and 17. Peak pressures for each of the researched fuels shown in Table 7 indicate that with the addition of IPK to the system, peak pressure increases.

The low DCN coupled with the higher volatility, smaller SMD, and greater LHV, produce significant engine knock. IPK resists autoignition and has an extended ID and CD meaning it ignites in the main combustion chamber after TDC when the air fuel mixture has time to become more homogeneous. This delayed combustion creates pronounced levels of engine knock which is reflected in the PRR shown in Figure 15.

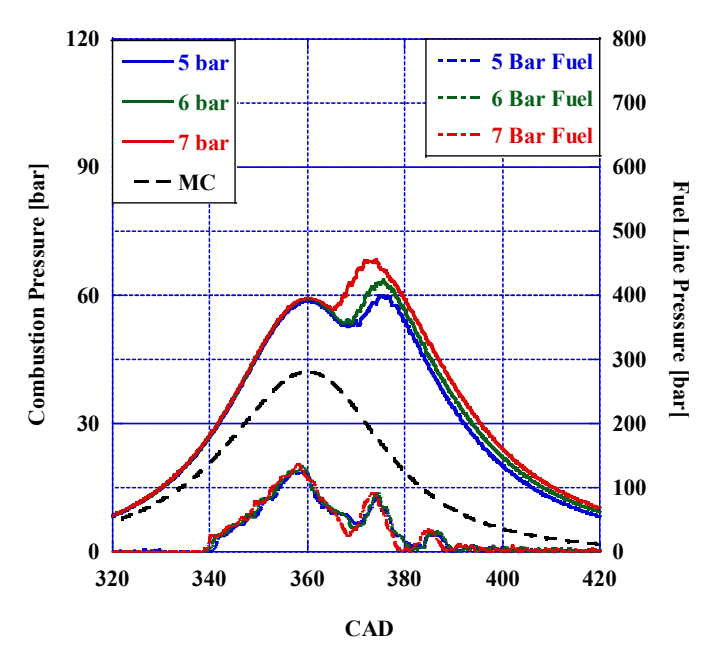


Figure 14: Combustion Pressure at 5, 6, and 7 bar IMEP for IPK

Figure 14 is the pressure curves for IPK at 5, 6, and 7 bar IMEP. It can be seen that the advanced ignition delay for the combustion of IPK is reduced at higher engine loads. This is due to increased pressure in the cylinder causing an increase in the DCN of the fuel [3]. At 7 bar IMEP, there can be seen the greatest difference in the ignition quality when compared to the other two loads. While there was in increase in combustion chamber pressure due to the higher load, there was a significant decrease in the ignition delay. Fuel line pressure remained practically the same for each load, however, there can be seen a greater drop in the fuel pressure after the initial peak pressure than can be seen at lower loads.

Furthermore, significant differences in fuel line pressure were found at 7 bar IMEP for each of the fuels. Figure 15 is a representation of the fuel line pressure around the peak pressure. It was found that the pressure in the fuel lines leading to injection was much lower for IPK than for ULSD with the blend falling between the neat fuels. This is due to the significant difference in the viscosity of IPK when compared to ULSD. Because IPK has a lower viscosity, the pressure that can be built in the lines is reduced as well as the amount the needle needs to move to allow the fuel to pass through. The thinner fuel can pass more fuel through a smaller opening in the injector needle than a thicker fuel. This results in a lower pressure built behind the needle and a reduction in the intensity of the oscillations in pressure after injection.

Additionally, the smaller orifice size due to the reduction in motion of the injector needle coupled with the reduced density and viscosity of IPK create ideal conditions for finer spray droplets more ideal for combustion.

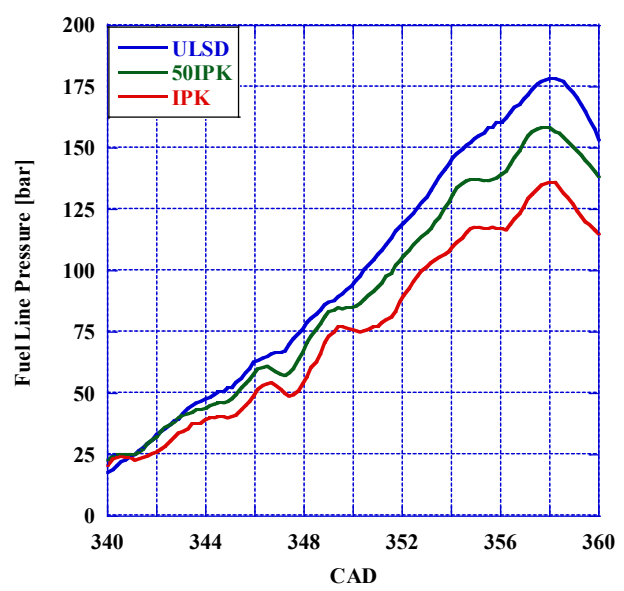


Figure 15: Fuel Line Pressure at Injection for ULSD, 50IPK50ULSD, and IPK

The peak pressures for each of the researched fuels in the fuel line can be seen in Table 8. ULSD reached the highest peak pressure at 178.52 bar while IPK reached a max pressure at 135.92 bar. The blend fell between these two values at 158 bar.

Table 8: Peak Fuel Line Pressures at 7 bar IMEP

Researched Fuel	Peak Fuel Line Pressure [bar]
ULSD	178.52
50ULSD50IPK	158.37
IPK	135.92

Presented in Figure 16 is the Pressure Rise Rate (PRR) of each of the researched fuels at 7 bar IMEP. It can be seen from this graph that there is a delay in the increase in PRR consistent with the ignition delay seen in Figures 13 and 14 for IPK. Additionally, PPRR (Peak Pressure Rise Rate) is significantly greater for IPK than for either ULSD or the blend. This dramatic spike in the PPRR in addition to the extended ignition delay cause IPK to have a significant amount of knock during combustion as seen in Figure 16.

The occurrence of knock is primarily due to the autoignition of unburned mixture in the end gas in the combustion chamber ahead of the propagating flame [30]. In this case, this high level of engine knock is due to the low DCN of IPK indicating its resistance to autoignition.

Peak Pressure Rise Rates for each of the researched fuels can be seen in Table 9. IPK was found to have the highest PPRR at 7.7 bar/CAD occurring at 368.1 CAD. This is due to lower autoignition quality of IPK when compared to ULSD

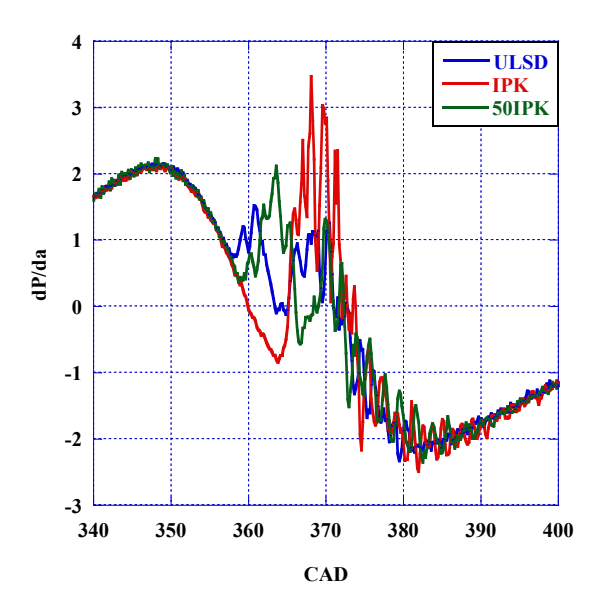


Figure 16: Change in Pressure vs CAD at 7 bar IMEP

causing a delay in the ignition and a sharp spike in pressure after the piston reaches Top Dead Center (TDC). The 50ULSD50IPK blend was found to have the lowest PPRR at 3.28 bar/CAD. This drastic increase in the PRR for IPK when compared to either the blend or to neat ULSD indicates severe levels of engine knock.

Table 9: Peak Pressure Rise Rates for Each Researched Fuel

Researched Fuel	Peak Pressure Rise Rate [bar/CAD]
ULSD	2.16
50ULSD50IPK	2.23
IPK	3.47

Apparent Heat Release Rate

The Apparent Heat Release Rate for this engine is calculated using Eq. 4. This equation works on the first principle of thermodynamics and can be solved with a few key assumptions: the working fluid acts as an ideal gas, is homogeneous, and the system undergoes no mass transfer during each cycle while the valves are closed.

$$\frac{dQ}{d\theta} = \frac{1}{(\gamma - 1)} V \frac{dP}{d\theta} + \frac{\gamma}{(\gamma - 1)} P \frac{dV}{d\theta} \tag{4}$$

The AHRR for each of the researched fuels at 7 bar IMEP can be seen in Figure 17. For ULSD and for the 50ULSD50IPK blend, there can be two distinct stages of combustion immediately following TDC, one is associated with ignition in the triple vortex chamber and the following stage represents the expulsion of the flames and unburned mixture from the high vortex chamber into the main combustion chamber. The two combustion stages are seen distinctively in the AHRR curve for the 50ULSD50IPK blend and neat ULSD. This combustion phenomenon, however, cannot be seen in the AHHR

curve for IPK. This is because the combustion event is delayed to well past TDC, and ignition occurs after the air fuel mixture is drawn into the main combustion chamber. IPK was also found to have a greater peak AHRR at 35.48 J/deg compared to ULSD at 22.32 J/deg. The peak AHRR for each of the researched fuels are displayed in Table 10.

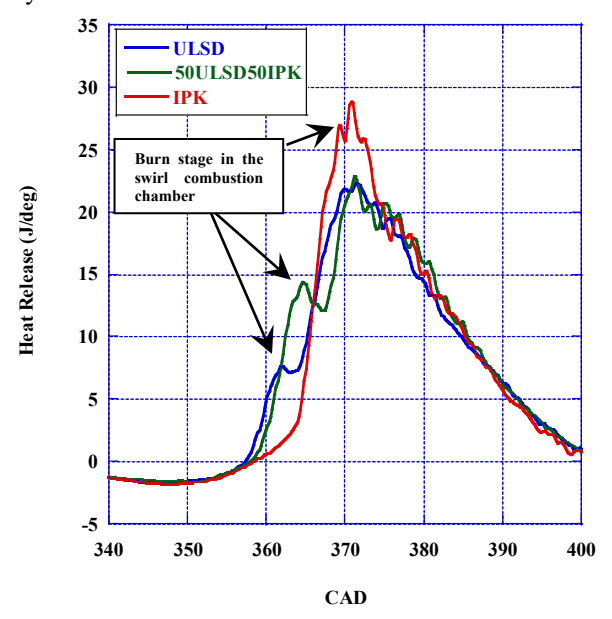


Figure 17: AHRR at 7 bar IMEP Table 10: Peak AHRR for the Researched Fuels

Researched Fuel	AHRR [J/CAD]
ULSD	22.32
50ULSD50IPK	22.84
IPK	35.48

RINGING INTENSITY

The Ringing Intensity (RI) at 7 bar IMEP was calculated for each of the researched fuel using Eq. 5. The β value was determined from literature to be 0.05 [32].

$$I = \frac{(\beta (\frac{dP}{dt})_{max})^2}{(2\gamma P_{max})} \sqrt{\gamma R T_{max}}$$
 (5)

IPK was found to have the highest RI at 15.23 consistent with its much greater PPRR when compared to the other researched fuels. Furthermore, it can be seen that with the addition of 50% my mass IPK to ULSD, there is a decrease in RI by approximately half when compared to ULSD. This determination is displayed in Figure 18.

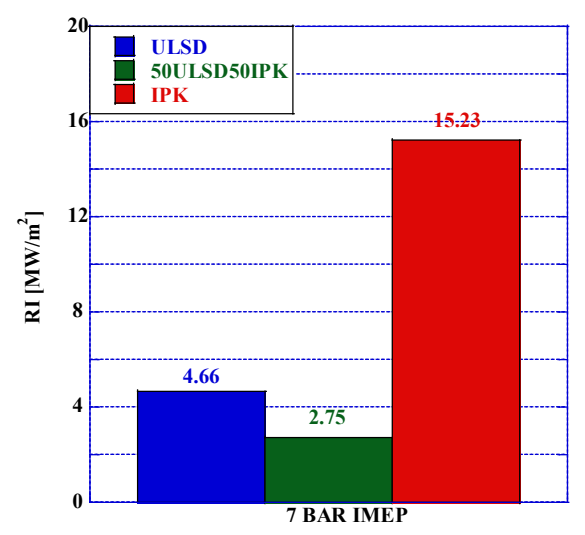


Figure 18: RI at 7 bar IMEP for Each of the Researched Fuel

EMISSIONS ANALYSIS

A study on the emissions produced by neat ULSD and a by mass blend of 50ULSD50IPK as a measure of the viability of alternative fuels for use in reducing harmful GHG emissions. This analysis was conducted using an MKS FTIR 2030 gaseous species analyzer. It was found that, for regulated emissions of CO, NO, and UHC, there was a significant reduction the levels produced from combustion for the 50ULSD50IPK blend. CO₂ levels, however, were found to increase when running the IPK/ULSD blend. Results for the NO, % CO₂, Unburned Hydrocarbons (UHC), and the CO emissions can be seen in Figures 19 and 20. In all cases, there was a significant reduction in the emissions produced by the combustion of 50ULSD50IPK when compared to ULSD at 7 bar IMEP.

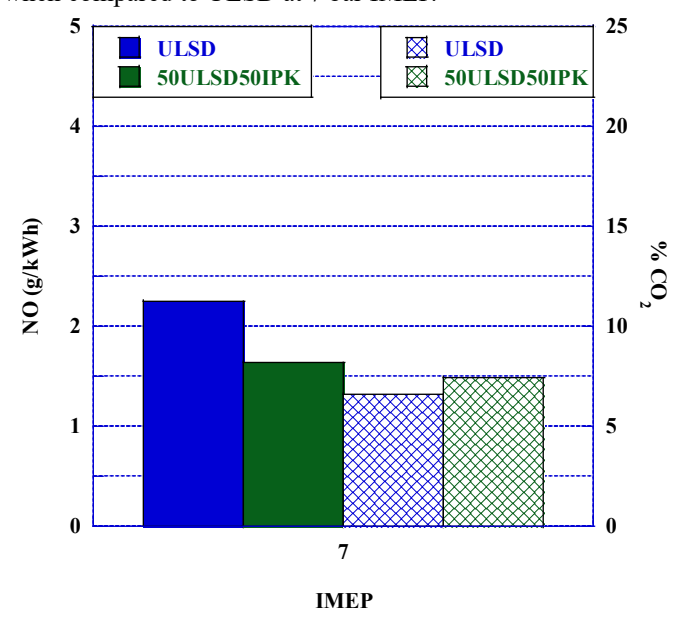


Figure 19: NO and % CO₂ Emissions for ULSD and 50ULSD50IPK at 7 bar IMEP

Data is converted to grams of the given species per kilowatt hour with the exception of CO₂ which is given in %.

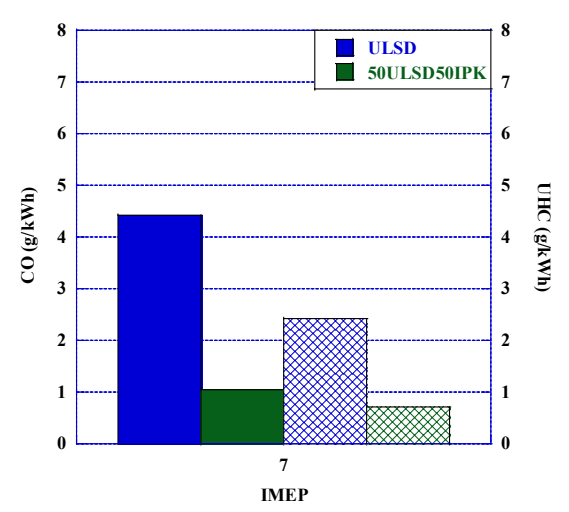


Figure 20: CO and UHC for ULSD and 50ULSD50IPK at 7 bar IMEP

CONCLUSION

An investigation was conducted on the thermophysical properties, combustion characteristics, and emissions profile on Fischer-Tropsch Iso-Paraffinic Kerosene (IPK) in a CVCC and an IDI CI engine as well as a by mass blend of 50% ULSD and 50%IPK. Combustion pressure, AHRR, and PRR were determined at 5, 6, and 7 bar IMEP. The thermophysical properties for IPK indicated that the fuel is more volatile and less viscous than either the blend or neat ULSD resulting in the finest spray pattern of the researched fuels. These properties indicated that IPK has theoretically favorable characteristics for rapid and complete combustion. The CVCC investigation, however, indicated that the combustion of IPK is much more delayed than that of ULSD or the 50ULSD50IPK blend because of the low DCN of IPK at 25.88 when compared to ULSD at 47. This reduction in the autoignition quality coupled with the favorable thermophysical properties contribute to the increased levels of knock when run in the IDI CI engine. It was found in the engine, that for neat IPK, there was a significant increase in engine knock. This can be attributed to the longer ID for IPK when compared to ULSD. It was found that the ID for IPK at 7 bar IMEP was 1.1 ms compared to ULSD at 0.88 ms. Additionally. peak pressure rise rate for IPK was the highest at 7.7 bar/CAD compared to ULSD at 4.29 bar/CAD. The 50ULSD50IPK blend, however, had the lowest PPRR at 3.28 bar/CAD indicating that its combustion produced the least knock. Additionally, ringing intensity for IPK at 7 bar IMEP was found to be double that of ULSD at 15.23 and 4.66, respectively. Following the analysis for PPRR, the 50ULSD50IPK blend had the lowest RI at 2.75. Because of the significant levels of engine knock, a by mass blend of 50% IPK and 50% ULSD was used to study the emissions output. It was found that the blend saw a significant reduction in NO, UHC, and CO emissions at 7 bar IMEP with an increase in the CO₂. While the combustion of neat IPK caused significant levels of engine knock, the additional of 50% ULSD both emissions and knock were greatly reduced.

ACKNOWLEDGEMENTS

We acknowledge the contribution of the Air Force Research Laboratory for suppling the experimental fuels, Christopher Mileski, Charles McGuffy, Michael Rankin, Jacques Lapeyre, from PACLP, Joseph von Wolfgang from Malvern Lasers, and Coty Harrison from Yokogawa. This paper is based upon work supported by the National Science Foundation Grant No. 1950207.

REFERENCES

- [1] C. E. D. Riboldi, "An optimal approach to the preliminary design of small hybrid-electric aircraft," *Aerospace Science and Technology*, vol. 81, pp. 14–31, 2018.
- [2] R. G. D. Santos and A. C. Alencar, "Biomass-derived syngas production via gasification process and its catalytic conversion into fuels by Fischer Tropsch synthesis: A review," International Journal of Hydrogen Energy, 2019.
- [3] V. Soloiu, R. Gaubert, J. Moncada, J. Wiley, J. Williams, S. Harp, M. Ilie, G. Molina, and D. Mothershed, "Reactivity controlled compression ignition and low temperature combustion of Fischer-Tropsch Fuel Blended with n-butanol," Renewable Energy, vol. 134, pp. 1173–1189, 2019.
- [4] C. Atkinson, G. Thompson, M. Traver, and N. Clark, "In-Cylinder Combustion Pressure Characteristics of Fischer-Tropsch and Conventional Diesel Fuels in a Heavy-Duty CI Engine," SAE Transactions, vol. 108, pp. 813–836, 1999.
- [5] Y. Jiao, R. Liu, Z. Zhang, C. Yang, G. Zhou, S. Dong, and W. Liu, "Comparison of combustion and emission characteristics of a diesel engine fueled with diesel and methanol-Fischer-Tropsch diesel-biodiesel-diesel blends at various altitudes," Fuel, vol. 243, pp. 52–59, 2019.
- [6] S. Jürgens, P. Oßwald, M. Selinsek, P. Piermartini, J. Schwab, P. Pfeifer, U. Bauder, S. Ruoff, B. Rauch, and M. Köhler, "Assessment of combustion properties of non-hydroprocessed Fischer-Tropsch fuels for aviation," Fuel Processing Technology, vol. 193, pp. 232–243, 2019.
- [7] S. S. Gill, A. Tsolakis, K. D. Dearn, and J. Rodríguez-Fernández, "Combustion characteristics and emissions of Fischer–Tropsch diesel fuels in IC engines," Progress in Energy and Combustion Science, vol. 37, no. 4, pp. 503–523, 2011.

- [8] H. Wang and M. A. Oehlschlaeger, "Autoignition studies of conventional and Fischer-Tropsch jet fuels," Fuel, vol. 98, pp. 249–258, 2012.
- [9] V. Soloiu, C. J. Phillips, C. Carapia, A. Knowles, D. Grall, and R. Smith, "Exploratory Investigation of Combustion and NVH Signature of a Drone Jet Engine Fueled with IPK," AIAA Scitech 2021 Forum, 2021.
- [10] Jinwoo Lee, Choongsik Bae, Application of JP-8 in a heavy duty diesel engine, Fuel, Volume 90, Issue 5, 2011, Pages 1762-1770, ISSN 0016-2361,
- [11] Alhikami, C.-E. Yao, and W.-C. Wang, "A study of the spray ignition characteristics of hydro-processed renewable diesel, petroleum diesel, and biodiesel using a constant volume combustion chamber," *Combustion and Flame*, vol. 223, pp. 55–64, 2021.
- [12] "Laser diffraction," *Sympatec*. [Online]. Available: https://www.sympatec.com/en/particle-measurement/glossary/laser-diffraction/. [Accessed: 13-Mar-2022].
- [13] S. Manigandan, P. Gunasekar, S. Poorchilamban, S. Nithya, J. Devipriya, and G. Vasanthkumar, "Effect of addition of hydrogen and TIO2 in gasoline engine in various exhaust gas recirculation ratio," *International Journal of Hydrogen Energy*, vol. 44, no. 21, pp. 11205–11218, 2019.
- [14] W. Zeng, M. Sjöberg, D. L. Reuss, and Z. Hu, "High-speed PIV, Spray, combustion luminosity, and infrared fuel-vapor imaging for probing tumble-flow-induced asymmetry of gasoline distribution in a spray-guided stratified-charge Disi engine," *Proceedings of the Combustion Institute*, vol. 36, no. 3, pp. 3459–3466, 2017.
- [15] J. T. Farrell, N. P. Cernansky, F. L. Dryer, C. K. Law, D. G. Friend, C. A. Hergart, R. M. McDavid, A. K. Patel, C. J. Mueller, and H. Pitsch, "Development of an experimental database and kinetic models for surrogate diesel fuels," SAE Technical Paper Series, 2007.
- [16] Zhang, C., Hui, X., Lin, Y., & Sung, C.-J. (2016). Recent development in studies of alternative jet fuel combustion: Progress, challenges, and opportunities. Renewable and Sustainable Energy Reviews, 54, 120–138. https://doi.org/10.1016/j.rser.2015.09.056
- [17] K. C. Kalvakala, P. Pal, J. P. Gonzalez, C. P. Kolodziej, G. Kukkadapu, S. Wagnon, R. Whitesides, N. Hansen, and S. K. Aggarwal, "Numerical Analysis of soot emissions from gasoline-ethanol and gasoline-butanol 1 blends under gasoline compression ignition conditions," SSRN Electronic Journal, 2022.
- [18] S. Yousuffuddin "Effect of combustion duration on the operating and performance characteristics of hydrogenethanol dual fueled engine: an experimental analysis" *Int. J. Adv. Autom. Technol.*, 1 (1) (2017), pp. 36-45
- [19] Alhikami, C.-E. Yao, and W.-C. Wang, "A study of the spray ignition characteristics of hydro-processed renewable diesel, petroleum diesel, and biodiesel using a constant

- volume combustion chamber," *Combustion and Flame*, vol. 223, pp. 55–64, 2021.
- [20] V. Soloiu, C. E. Carapia, R. Smith, A. Weaver, L. Mckinney, D. Mothershed, D. Grall, M. Ilie, and M. Rahman, "RCCI with high reactivity S8-ULSD blend and low reactivity N-Butanol," ASME 2020 Internal Combustion Engine Division Fall Technical Conference, 2020
- [21] Soloiu, V., Weaver, A., Parker, L., Brant, A., Smith, R., Ilie, M., Molina, G., Carapia, C. (2022). Constant Volume Combustion Chamber (CVCC) Investigations of Aerospace F-24 and Jet-A in Low-Temperature Heat Release and Negative Temperature Coefficient Regions. Energy Conversion and Management, 263, 115687. https://doi.org/10.1016/j.enconman.2022.115687
- [22] S. Cheng, D. Kang, A. Fridlyand, S. S. Goldsborough, C. Saggese, S. Wagnon, M. J. McNenly, M. Mehl, W. J. Pitz, and D. Vuilleumier, "Autoignition behavior of gasoline/ethanol blends at engine-relevant conditions," Combustion and Flame, vol. 216, pp. 369–384, 2020.
- [23] S. Cheng, C. Saggese, D. Kang, S. S. Goldsborough, S. W. Wagnon, G. Kukkadapu, K. Zhang, M. Mehl, and W. J. Pitz, "Autoignition and preliminary heat release of gasoline surrogates and their blends with ethanol at engine-relevant conditions: Experiments and comprehensive kinetic modeling," Combustion and Flame, vol. 228, pp. 57–77, 2021.
- [24] Heywood, J. 1988, Internal Combustion Engine Fundamentals, McGraw-Hill, New York.
- [25] A Methodology for Cycle-By-Cycle Transient Heat Release Analysis in a Turbocharged Direct Injection Diesel Engine, 2000.
- [26] V. Soloiu, T. Naes, M. Muinos, S. Harp, J. Moncada, R. Gaubert, and G. Molina, "Comparison of combustion and emissions properties of jet-A vs. ULSD in both indirect and direct compression ignition engines at same IMEP," SAE Technical Paper Series, 2016-01-0733, DOI: 10.4271/2016-01-0733.
- [27] V. Soloiu, D. Nelson, A. Covington, and J. Lewis, "Investigations of a fatty acid methyl ester from poultry fat in a triple vortex separate combustion chamber diesel engine stage one-combustion investigations," *SAE Technical Paper Series*, 2011-01-1188, DOI: https://doi.org/10.4271/2011-01-1188.
- [28] V. Soloiu, J. Moncada, M. Muinos, A. Knowles, R. Gaubert, T. Beyerl, and G. Molina, "Performance evaluation combustion, emissions and vibrations-of n-butanol binary mixture with ULSD in an indirect injection engine," SAE Technical Paper Series, 2017-01-0875, DOI: 10.4271/2017-01-0875.
- [29] V. Soloiu, S. Harp, C. Watson, M. Muinos, S. Davoud, G. Molina, B. Koehler, J. Heimberger, M. Jansons, and C. Butts, "Performance of an IDI engine fueled with fatty acid methyl esters formulated from cotton seeds oils," SAE International Journal of Fuels and Lubricants, vol.

- 8, no. 2, pp. 277–289, 2015-01-0806, DOI: 10.4271/2015-01-0806.
- [30] V. Soloiu, R. Gaubert, M. Muinos, J. Moncada, T. Beyerl, G. Molina, and J. Williams, "Performance of an indirect injected engine operated with ULSD#2 blended with Fischer-Tropsch synthetic kerosene," *SAE Technical Paper Series*, 2017-01-1283, DOI: 10.4271/2017-01-1283.
- [31] S. Gersen, M. van Essen, H. Levinsky, and G. van Dijk, "Characterizing gaseous fuels for their knock resistance based on the chemical and physical properties of the Fuel," *SAE International Journal of Fuels and Lubricants*, vol. 9, no. 1, pp. 1–13, 2016.
- [32] J. A. Eng, "Characterization of pressure waves in Hcci Combustion," SAE Technical Paper Series, 2002